JOURNAL OF SPACECRAFT AND ROCKETS
Vol. 38, No. 3, May–June 2001

Modeling of Spacecraft–Environment Interactions on SMART-1

M. Tajmar*
Austrian Research Centers Seibersdorf, A-2444 Seibersdorf, Austria
and
J. González† and A. Hilgers‡
ESA, 2200 AG Nordwijk, The Netherlands

A three-dimensional numerical model was developed to investigate the interactions of a Hall thruster plume with the Small Missions for Advanced Research in Technology (SMART-1) spacecraft, which is the first of the SMART missions in the ESA Horizons 2000 Science plan. The main mission objective of SMART-1 is to demonstrate innovative and key technologies for scientific deep-space missions. One of these key technologies is the use of solar electric propulsion as primary propulsion. This technology demonstration mission will use a modified Stationary Plasma Thruster-100 (SPT-100) Hall thruster, which was already the subject of successful modeling using the particle-in-cell method. Based on these model approaches, the present model simulates the thruster plume together with the whole spacecraft, including parts of the solar array. Specifically, the present study concentrates on assessing contamination issues from charge-exchange ions. The model assumes a quasi-neutral plasma using collisionless electrons in which the magnetic field can be neglected. Because of the lack of measurements from the modified thruster, the model is verified using existing experimental data from the well-studied SPT-100. SMART-1 will feature several sensors to investigate spacecraft–environment interactions. Finally, the model is used to predict the plasma densities and ion currents that will be collected onboard the spacecraft.

Nomenclature

A	=	thruster exit area, m^2
B	=	magnetic field, T
E	=	electric field, Vm^{-1}
e	=	electric charge, 1.602×10^{-19} C
k	=	Boltzmann constant, 1.381×10^{-23} JK^{-1}
$\dot{m}$	=	mass flow rate, kgs^{-1}
n_{ref}, n_e, n_i	=	electron reference, electron, and ion number density, m^{-3}
p	=	pressure, Pa
T	=	thrust, N
T_e	=	electron temperature, eV
V_p	=	plasma potential, V
v_e, v_i, v_n	=	electron, ion, neutral and velocity, ms^{-1}
$W_{\text{ion}}, W_{\text{neutral}}$	=	ion and neutral test particle ratio, real atoms per test particle
Y	=	sputter yield, atoms per ion
η_a	=	propellant directed through anode, %
η_p	=	doubly charged ion percentage, %
η_u	=	propellant ionization efficiency, %
σ_{CEX}	=	charge-exchange cross section, m^{-2}
ϕ	=	potential, V
ϕ_f	=	spacecraft floating potential, V
ϕ_∞	=	reference potential at thruster exit, V

Introduction

THE first of the Small Missions for Advanced Research in Technology (SMART-1) of the ESA Horizons 2000 scientific program is dedicated to the testing of new technologies for preparing future cornerstone missions, using solar-electric propulsion in deep space. SMART-1 will be placed in orbit around the moon using a Hall thruster (PPS-1350) with a maximum thrust of 70 mN built by the Societe Europeen de Propulsion[1,2] and will be launched in 2002 as an Ariane 5 cycladelike auxilary payload.

This will be the first time using primary electric propulsion on a European spacecraft. Hence, the evaluation of the Hall thruster impact on the spacecraft and its instruments is one of the primary scientific objectives.[3] In addition to primary beam ions, electric propulsion thrusters create a low-energy charge-exchange ion environment. The distribution of these ions is strongly affected by the potential distribution near the spacecraft being a possible contamination source for instruments and solar arrays. Although charge-exchange plasma interactions have been a subject of extensive experimental and theoretical studies,[4–6] there have been few comprehensive in-flight investigations due to the lack of flight opportunities. The first interplanetary spacecraft using solar electric propulsion is Deep Space One,[6] using the NASA solar electric propulsion technology application readiness ion engine. SMART-1 will be the first interplanetary flight using a Hall thruster.

Hall thrusters have been extensively tested in vacuum chambers and abundant data are available to compare with numerical models.[7–11] Several models have been developed[12–14] obtaining good agreement between measurements and simulation. Whereas most models are two-dimensional axisymmetric, only the model from Oh and Hastings[12] enables three-dimensional and real spacecraft geometries. All previous models do not account for the real physical dimensions of the instruments such as the Langmuir probe or the retarding potential analyzer. However, this is especially necessary if large gradients appear in the data as shown by measurements.[9]

Two payload experiments, the electric propulsion diagnostic package (EPDP) and the Spacecraft Potential, Electron and Dust Experiment, including Langmuir probes and a retarding potential analyzer, are dedicated to measure the ambient plasma variables during the operation of the Hall thruster. The Austrian Research Centers Seibersdorf, together with the European Space and Research Technology Centre (ESTEC), is currently developing modeling tools to predict and help to interpret instrument data to study spacecraft–environment interactions on SMART-1. This paper presents a three-dimensional hybrid particle-in-cell[15,16] Monte Carlo collisions (PIC–MCC) model to predict the charge-exchange ion environment. Ions and neutrals are treated as test particles, whereas the electrons are assumed to follow a Boltzmann distribution described in a collisionless, isothermal electron momentum equation. By neglecting the magnetic field and assuming a

Received 12 April 2000; revision received 1 September 2000; accepted for publication 5 January 2001.

*Staff Member, Space Propulsion Section; martin.tajmar@arcs.ac.at.
†Staff Member, European Space Research and Technology Centre, Electric Propulsion Section, P.O. Box 299; Jose.Gonzalez@esa.int.
‡Staff Member, European Space Research and Technology Centre, Space Environments and Effects Analysis Section, P.O. Box 299; Alain.Hilgers@esa.int.

quasi-neutral plasma, one is able to derive the potential distribution. Simulations of a Hall thruster in real spacecraft geometries with virtual plasma sensors of specified dimensions are presented. The virtual sensors, combined with a full three-dimensional environment and a momentum conserving MCC method, sets this simulation approach apart from previously published models by Oh and Hastings,[12] VanGilder and Boyd,[13] VanGilder et al.,[13] and Bareilles et al.[17] The code has been tested against several ground measurements and shows good agreement, even on a linear scale. Predictions of the plasma environment around SMART-1 and sensor data from the EPDP instruments are presented and discussed.

Physical Model

A Hall thruster emits an ion beam out of a ring-shaped anode with a half-angle divergence of about 40 deg. Typical operating parameters are summarized in Table 1. A schematic setup is shown in Fig. 1. Electrons from an external cathode act as a neutralizer, creating a quasi-neutral plasma. Although the propellant efficiency for these type of thrusters exceeds 95%, the neutral density is comparable to the beam ion density due to the much lower thermal velocities (400 m/s) compared to the ion velocities gained due to the acceleration potential of 350 V (22,500 m/s). Moreover, part of the propellant is directed through the cathode, thus providing an additional flow of neutral propellant.

Theoretical considerations[18] and measurements by King[10] suggest that most of the high-energy ions will be formed close to the inner wall of the anode ring. To leave the anode without colliding with the walls, the ion beam will be directed more outward from the center of the anode (Fig. 2). The divergence angle going from λ_{left} to λ_{right} was found to vary linearly with radial position.[7,19] About 10–20% of the ions are doubly charged, depending on the type of Hall thruster.[8]

Table 1 PPS-1350 performance parameters

Parameter	Value
Thrust	70 mN
Voltage	350 V
Current	3.8 A
Mass flow rate	4.2 mg/s
Specific impulse	1640 s
Power	1350 W
Total efficiency	51%
Divergence angle	42 deg
Outer insulator diameter	100 mm
Inner insulator diameter	56 mm

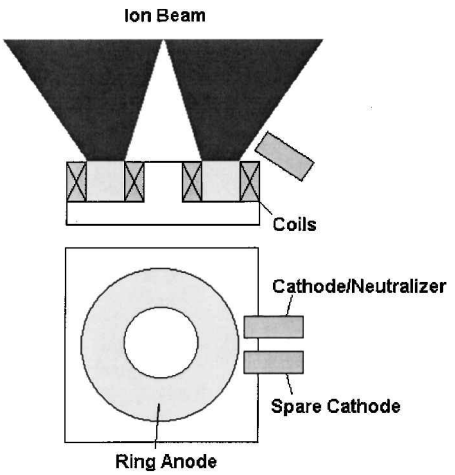

Fig. 1 Hall thruster schematic setup.

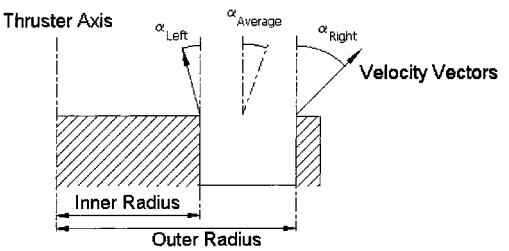

Fig. 2 Ion beam velocity vectors at the thruster's exit.

To express the mass flow rate and the velocities of the singly and doubly charged ions ($\dot{m}_i^+, \dot{m}_i^{++}, v_i^+, v_i^{++} = \sqrt{2} \cdot v_i^+$) at the thruster's exit, we will use the following relationships:

$$T = \left(\dot{m}_i^+ \cdot v_i^+ + \dot{m}_i^{++} \cdot \sqrt{2} \cdot v_i^+\right) \cdot (\sin\alpha_{\text{av}}/\alpha_{\text{av}})^2 \tag{1}$$

$$\dot{m} \cdot \eta_u \cdot \eta_a = \dot{m}_i^+ + \dot{m}_i^{++} \tag{2}$$

$$n_i^{++} = \frac{\dot{m}_i^{++}}{A \cdot \sqrt{2} \cdot v_i^+} = \eta_p \cdot \frac{\dot{m}_i^+}{A \cdot v_i^+} = \eta_p \cdot n^+$$

$$\Rightarrow \dot{m}_i^{++} = \eta_p \cdot \sqrt{2} \cdot \dot{m}_i^+ \tag{3}$$

where T is the thrust, $\dot{m}$ the total mass flow, $\alpha_{\text{av}} = (\alpha_{\text{left}} + \alpha_{\text{right}})/2$ to account for geometric losses, η_u is the ionization efficiently, η_a the percentage of propellant directed through the anode, and η_p the percentage of doubly charged ions. Hence, the ion exit conditions are

$$v_i^+ = \frac{T \cdot \left(1 + \eta_P \cdot \sqrt{2}\right)}{\dot{m} \cdot \eta_u \cdot \eta_a \cdot (1 + \eta_P \cdot 2) \cdot (\sin\alpha_{\text{av}}/\alpha_{\text{av}})^2} \tag{4}$$

$$\dot{m}_i^+ = \frac{T}{v_i^+ \cdot (1 + \eta_P \cdot 2) \cdot (\sin\alpha_{\text{av}}/\alpha_{\text{av}})^2} \tag{5}$$

The mass flow rate of the doubly charged ions can be calculated accordingly. Axial and radial temperatures are added to the ion beam velocity according to measurements[7,19] when a Maxwellian distribution is assumed. The distribution of ions along the anode exit is assumed to be homogeneous.

The neutrals are assumed to follow a cosine distribution at thermal velocities with a temperature of 1000 K, which is in good agreement with experiments of a similar Hall thruster.[20] They originate both from the anode and cathode as given by the neutral mass flow rates

$$\dot{m}_{\text{na}} = \dot{m} \cdot (1 - \eta_u) \cdot \eta_a, \qquad \dot{m}_{\text{nc}} = \dot{m} \cdot (1 - \eta_a) \tag{6}$$

Electrons have much higher velocities than ions due to their lower mass. Hence, full particle PIC simulations require very small time steps and smaller artificial ion masses to solve the numerical problem in the timescales of days on standard personal computer workstations.[21] In the hybrid PIC model, the electrons are modeled through the electron momentum equation rather than particles, which is computationally much faster:

$$m_e n_e \frac{\mathrm{d}v_e}{\mathrm{d}t} = -n_e e(E + v_e \times B) - \nabla p - n_e m_e \nu_{\text{ei}}(v_e - v_i) \tag{7}$$

where ν_{ei} is the collision frequency between electrons and ions and p the pressure. This approach is similar the models from Oh and Hastings and VanGilder and Boyd.[13] For the plasma densities and temperatures produced by a Hall thruster, the electrons can be treated as collisionless.[12] Moreover, we can also neglect the magnetic fields to obtain very good comparisons between simulation and experiments.[12,13] Neglecting the left-hand side due to the very small electron mass, we are left with

$$n_e e E = \nabla p \tag{8}$$

In a perfect gas, assuming isothermal conditions, one obtains the Boltzmann relationship to express the electron density. Experiments[9] also show that the electron density is following the ion density to a very good extent. Hence, we can assume quasi-neutral plasma conditions and finally arrive at

$$n_i \approx n_e = n_{\text{ref}} \cdot \exp(e\phi/kT_e) \tag{9}$$

where T_e is the electron temperature, ϕ the potential, and n_{ref} the reference electron density where the potential is set to zero. In our simulations, the exit ion density and the exit potential measured by

Haas and Gallimore[22] is used to calculate n_{ref}. As a simplification, a fixed electron temperature T_e is assumed throughout the whole simulation domain similar to Oh and Hasting's[12] model. This is not true in reality because measurements[9] indicate a relationship between the strong varying ion density and the electron temperature. However, the ion density quickly (>20 cm from the thruster's exit) becomes much more homogeneous and the electron temperature follows this trend accordingly. Because we are more interested in the influence of the Hall thruster in the spacecraft environment and not specifically near the thruster's exit, the fixed electron temperature model seems to be appropriate.

The sputter yield Y of the charge-exchange ions to a specific surface depends on the kinetic energy E modeled through the simple expression

$$Y = E \cdot s_1 - s_2 \tag{10}$$

where $s_1 = 1.275 \times 10^{-3}\ \mathrm{eV}^{-1}$ and $s_2 = 0.0675$ are the constants for aluminium as given by Rosenberg and Wehner[23] in the case of an ion hitting the spacecraft surface.

Numerical Model

A three-dimensionalhybrid PIC–MCC[15,16] model was developed treating the ions and neutrals as test particles and computing the potential from the ion density and the fixed electron temperature and reference electron density in Eq. (9), when a quasi-neutral plasma is assumed. At every time step dt, singly and doubly charged ions are injected at the thruster exit plane according to their mass flow rate and velocity, Eqs. (4) and (5). Similarly, propellant neutrals are injected at the anode and cathode according to the mass flow rate in Eq. (6). Their thermal velocity vector is randomly assigned from a cosine distribution.

The Hall thruster can be either modeled alone or on top of a cubic spacecraft with a solar array attached on the side (Fig. 3). The quasi-neutral assumption avoids having to solve Poisson's equation on the grid, and, hence, the gridsize is not limited by the plasma's debye length. This enables simulation of a large domain at a very high precision. With a standard 400-MHz workstation, a $2 \times 2 \times 2$ m domain using $100 \times 100 \times 100$ gridpoints and up to 1,000,000 particles could easily be calculated within one day.

Models by Oh and Hastings[12] and VanGilder and Boyd[13] apply the direct simulation Monte Carlo (DSMC) collision method to compute charge-exchange collisions between the ion and neutral beam. This model applies the classical Monte Carlo method, which is computationally faster and was shown to be equivalent to DSMC for Hall thruster models.[17] In this scheme, a probability of collision P is added at each time step dt to an ion particle:

$$P = 1 - \exp[-v_{\mathrm{relative}} \cdot \sigma_{\mathrm{CEX}} \cdot n_n(x, y, z) \cdot \mathrm{d}t] \tag{11}$$

where v_{relative} is the relative velocity between the ion and neutral beam, n_n the neutral density at the particle's position, and σ_{CEX} the collision cross section, which is derived from quantum theory expressed by

$$\sigma_{\mathrm{CEX}}(v_{\mathrm{relative}}) = (k_1 \ln v_{\mathrm{relative}} + k_2)^2 \tag{12}$$

where $k_1 = -0.882 \times 10^{-10}$ s and $k_2 = 1.513 \times 10^{-9}$ m for $Xe^+ - Xe$ according to Rapp and Francis[24] and $k_1 = -2.704 \times 10^{-10}$ s and $k_2 = 3.6 \times 10^{-9}$ m for $Xe^{++} - Xe$ collisions according to Oh and Hastings,[12] respectively. If P is greater than a random number R_n between 0 and 1, a collision occurs. Because the neutral test particle ratio is usually higher than the ion test particle ratio, another random number is chosen to decide if the momentum of the ion particle is exchanged with the closest neutral particle or if the ion particle velocity is reduced to thermal speeds without changing the ambient neutral density:

$$R_n < \frac{W_{\mathrm{ion}}}{W_{\mathrm{neutral}}} \Rightarrow \text{exchange momentum} \tag{13}$$

This conserves the momentum in the simulation. For ground-test code validations, the residual gas density of the vacuum chamber has to be included in the neutral density n_n in Eq. (11). Neutral propellant is assumed to be homogeneously distributed at room temperature according to the pressure inside the chamber, similar to the experiments of VanGilder and Boyd.[13]

Two different types of instruments are modeled to compare with ground-test data: a Faraday cup and a retarding-potential-analyzer. Both are implemented inside the simulation domain with their specific probe diameter. Every time step, ions are checked if they passed the instrument location, and the collected current is monitored. If an ion particle passes through the spacecraft surface, it contributes to the backflow current. At the same time, the sputter yield is calculated using Eq. (10)

Code Verification

Before calculating the SMART-1 environment, we will use ground-test data to verify the numerical simulation. Unfortunately, probe data for the PPS-1350 thruster have not been published. However, abundant data exist for the Stationary Plasma Thruster-100 (SPT-100) Hall thruster, which only differs slightly in the specific impulse and magnetic field. Apart from the difference in the magnetic field (which is neglected in the simulation) the main physical difference is the higher discharge potential of 350 V for the PPS-1350 thruster compared to the 300 V for the SPT-100. Hence, switching the discharge potential will enable us to simulate both type of thrusters.

The simulation parameters are given in Table 2. Figure 4 plots a comparison of horizontal Faraday cup sweeps with a probe diameter of 2.4 mm at distances of 10, 100, and 200 mm to characterize the near field. The domain size was chosen as $0.2 \times 0.2 \times 0.2$ m to resolve the probe diameter accuracy using a grid of $100 \times 100 \times 100$. The simulation follows the trends of the measurement at several horizontal distances to a good extent. Also, the quantitative agreement is reasonable. Only the sharp peak at 100 mm seems to be overpredicted by 100%. However, the data containing large gradients were obtained from an intrusive measurement, and the authors

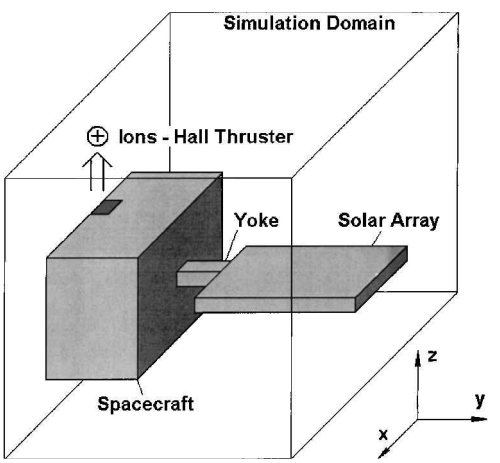

Fig. 3 Simulation setup.

Table 2 Code verification simulation parameters

Parameter	Simulation value
Grid	$100 \times 100 \times 100$
Background pressure	10^{-6} mbar
Thrust	84 mN
Mass flow rate	5.6 mg/s
Cathode position (X, Y, and Z)	85, 15, and 10 mm
Cathode diameter	7 mm
Cathode split η_c	10%
Doubly charged percentage η_P	10%
Ionization efficiency η_U	95%
Neutral temperature	1000 K
α_{left}	−12 deg
α_{right}	40 deg
Electron temperature T_e	4 eV
Reference potential Φ_∞	20 V

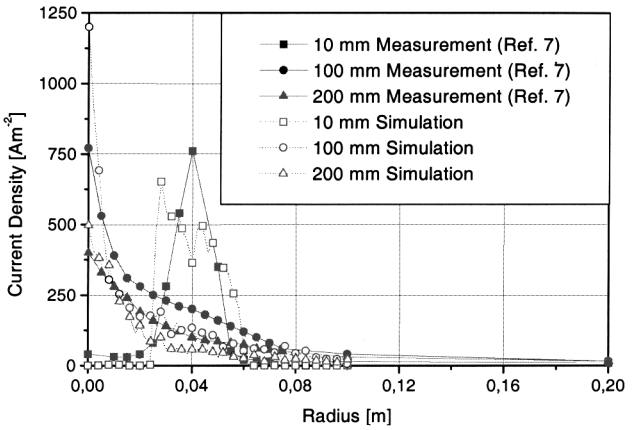

Fig. 4 Near-field Faraday cup comparison.

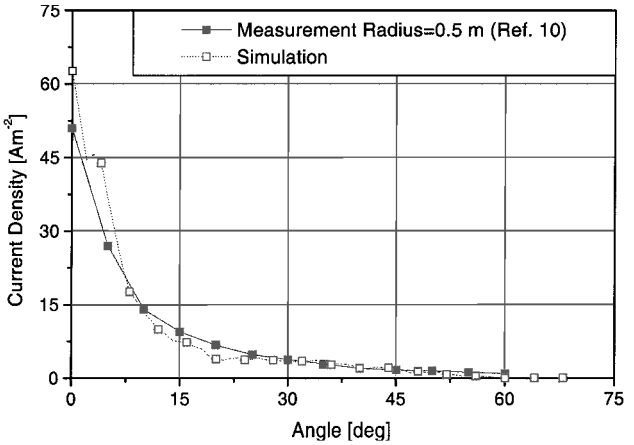

Fig. 5 Faraday cup comparison at $R = 0.5$ m.

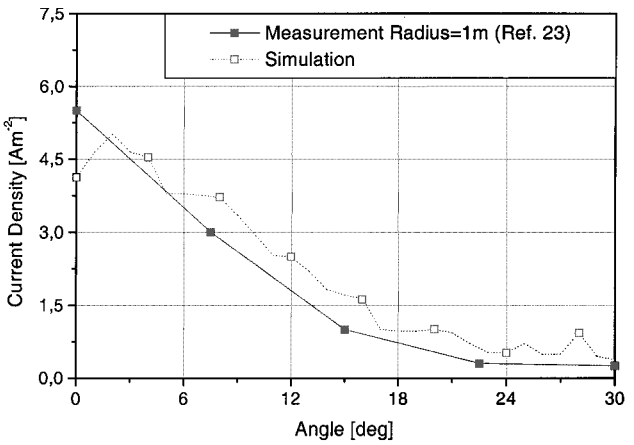

Fig. 6 Faraday cup comparison at $R = 1$ m.

report a discrepancy of the total current integrated along the thruster axis.

We next compare the far-field Faraday cup measurements with a probe diameter of 2.3 cm at horizontal distances of 0.5 and 1 m in Figs. 5 and 6, respectively.[10,25] Here, the domain size was set to $1 \times 1 \times 1$ m. The agreement is very good even on a linear scale (compared to other comparisons published on logarithmic scale[12,13]). During the simulation, the peak at 0 deg was very sensitive to the ion distribution at the exit and the α_{left} parameter. For example, introducing a Gaussian distribution[13] at the thruster's exit makes the peak even higher compared to the homogeneous case because more ions are emitted at smaller divergence angles, thus reaching the Faraday cup near the thruster axis. Similar behavior was found for α_{left}. If this parameter is increased, more ions reach the probe at

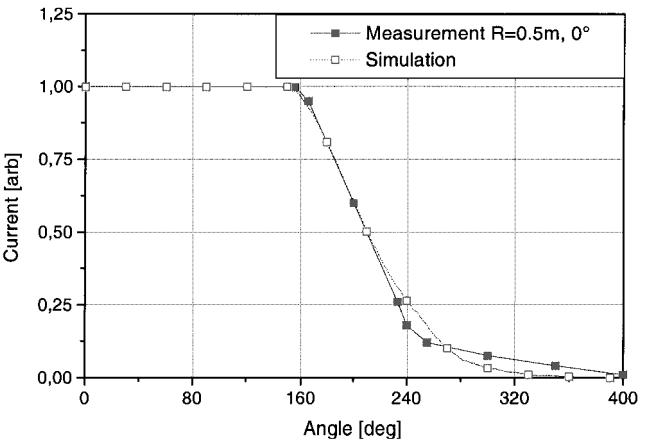

Fig. 7 Retarding-potential-analyzer comparison at $R = 0.5$ m.

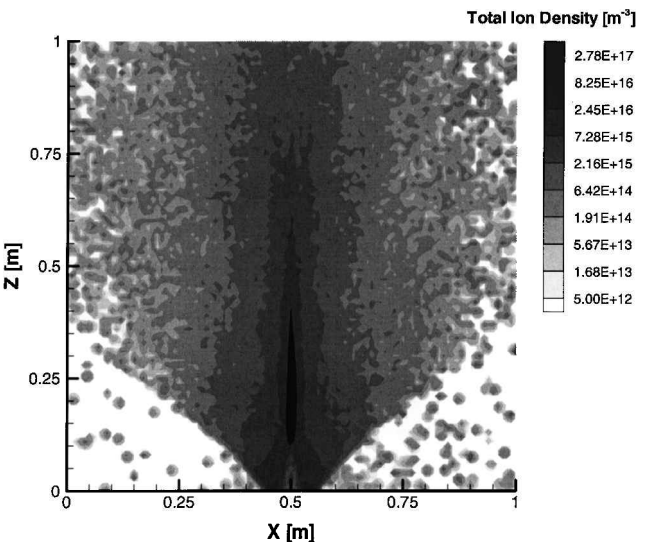

Fig. 8 Total ion density on x–z plane of PPS-1350 thruster at 70 mN.

the center, thus increasing the peak. The simulation parameters in Table 2 represent the best fit to match the experimental data.

Last, we compare the ion energies with data from a retarding potential analyzer at $R = 0.5$ m from the thruster z axis and 0 deg from the x axis in Fig. 7. The simulation agrees well with the data, indicating the correctness of our ion velocity model in Eq. (4). The simulation results that were most sensitive were the percentages of doubly charged ions and temperatures. A higher η_P of 10% as used in our simulation shifts the first knee in our data from 160 eV to lower energies. The temperatures influence the gradient of the plotted data. Again, our simulation parameters represent the best fit to the measurements available.

In our comparisons, we verified the ion currents and energies at various distances for a SPT-100 Hall thruster. The good agreement encourages to us apply our model to simulate the PPS-1350 thruster plume and to put it on a SMART-1 geometry to evaluate its plasma environment.

Spacecraft–Environment Interactions on SMART-1

Before evaluating the influence of the Hall thruster plume on the whole spacecraft, we will look at the ion and neutral densities from the thruster only on an x–y plane as shown in Figs. 8 and 9, respectively, that cuts through the middle of the spacecraft as shown in Fig. 3. The simulation domain was $1 \times 1 \times 1$ m with no background pressure, thus resembling a vacuum environment. In the neutral density plot, we clearly see the asymmetry due to the propellant flowing through the cathode located on the right side of the thruster. This influences the production of charge-exchange ions coming out from the primary ion beam, as shown in Fig. 8. Because

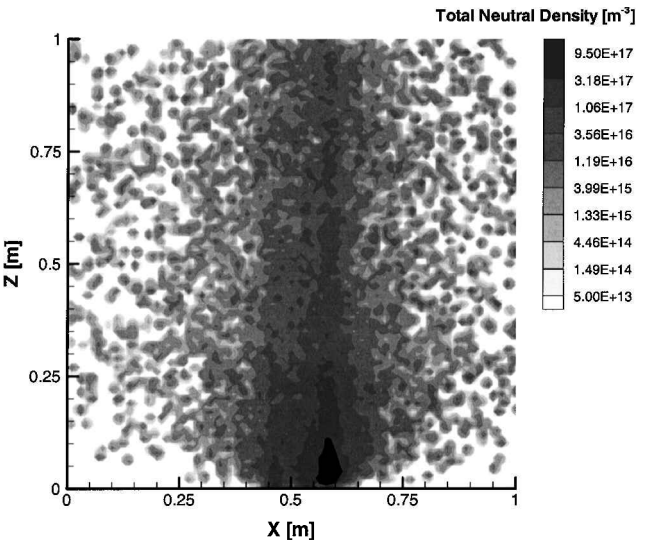

Fig. 9 Neutral density on x–z plane of PPS-1350 thruster at 70 mN.

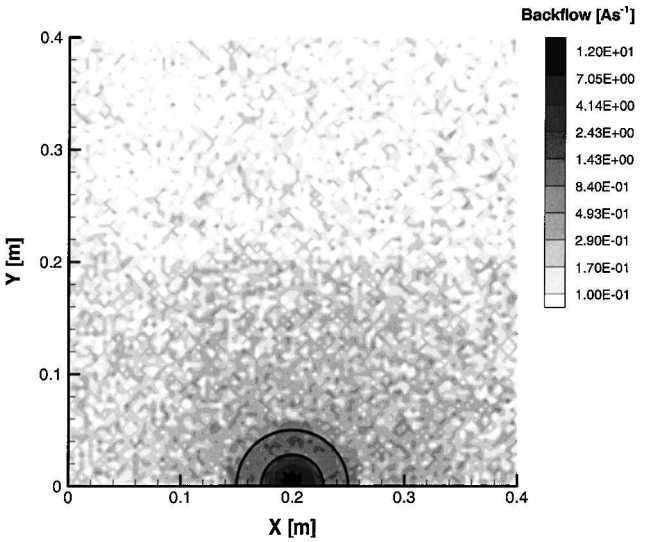

Fig. 10 Backflow on x–y plane at spacecraft surface (ring represents hall thruster anode).

most charge-exchange collisions will occur at locations where the ion and neutral densities are at their maximum, most of the collisions are expected to occur close to the thruster's exit ring and near the cathode. The slow ions, initially having only thermal velocities, will then follow the potential distribution around the thruster. In our physical model, we assumed a quasi-neutral plasma and derived the potential from the ion density. Looking at the ion density plot in Fig. 8, we note a maximum near the thruster's exit ring and a density build up at the thruster's axis 10 cm above the spacecraft surface. This is characteristic for a ring-type emission. Similar to the ion density buildup, a potential hump is also expected in our quasi-neutral plasma model. Hence, the charge-exchange ions below the potential hump will be deflected toward the spacecraft surface, and all other slow ions will be more radially deflected parallel to the spacecraft surface. Figure 10 plots the backflow structure on the surface using an even smaller domain size of $0.4 \times 0.4 \times 0.4$ m. Most backflow ions are concentrated on the inner ring thruster area. They originate from the ion density maximum at the thruster's exit, deflected by the potential hump and the positive space charge from the primary beam ions. On the right side of the peak, we also note an asymmetry due to the cathode's neutral density peak. Integrating the backflow current over the surface, we obtain $I_B = 3.51 \pm 0.16 \times 10^{-2}$ A, which is about 0.9% of the beam current (Table 1).

How does this current influence the spacecraft floating potential? Assuming a Boltzmann distributed ambient electron density

Table 3 SMART-1 domain parameters

Parameter	Simulation value
Domain size	$2 \times 2 \times 2$ m
Solar array (width, thickness)	1, 0.1 m
Yoke (length, diameter)	0.1, 0.1 m

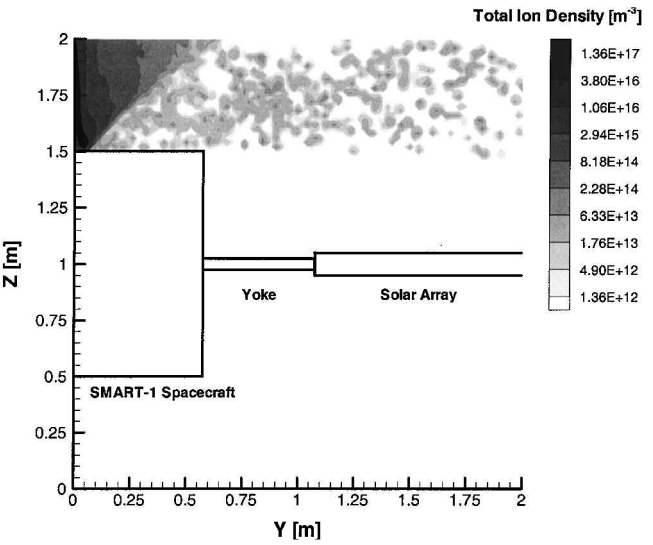

Fig. 11 Total ion density on y–z plane of SMART-1 at 70 mN thrust.

that equals the backflow current to give the change in the floating potential, a simple estimate can be written as

$$\Delta\phi_f = \frac{4 \cdot I_B \cdot k \cdot T_e}{e^2 \cdot n_e \cdot \sqrt{8 \cdot k \cdot T_e/\pi \cdot m_e}} \tag{14}$$

Using Eq. (14) to compute the potential change in an ambient low-Earth-orbit (LEO) plasma ($T_e = 0.1$ eV, $n_e = 1 \times 10^{12}$ m^3) yields $\phi_f = 0.41$ V. The LEO plasma case represents the worst case because SMART-1 will be injected much higher in a geostationary transfer orbit. Even this thruster-induced floating potential in a LEO plasma is very small compared to floating potentials due to the solar wind or the magnetosheath ($\phi_f = 2$–10 V) as listed in Ref. 26, which is representative for interplanetary space and the SMART-1 mission trajectory.[3] Hence, at least using this simple estimate, the operation of a Hall thruster does not cause significant changes in the spacecraft floating potential.

We now apply our simulation on the SMART-1 geometry. The spacecraft cube has the dimensions $1.15 \times 1.15 \times 1$ m and has two solar arrays stretching out from two opposite sides, giving a total length of 8 m. To include at least part of the solar array, the domain size was $2 \times 2 \times 2$ m. The solar array can rotate around the y axis during flight to maintain a maximum solar flux. This was not implemented in the simulation and only one fixed position, as shown in Fig. 3, was assumed. The geometry parameters are summarized in Table 3.

Figure 11 shows the ion density on an x–z plane through the middle of the thruster and the SMART-1 spacecraft, including the solar arrays. The initial beam divergence of the primary beam ions is clearly evident. In this plot, the maximum ion density hump at the thruster's exit reaches a value of 1×10^{17} m^{-3}. As outlined, the backflow ions form a cone close to the thruster's geometry. Other charge-exchange ions radially leave the beam, creating an ion density almost four orders of magnitude less than at the thruster's exit. Most important, the ion's space charge seems not to be sufficient to expand the ion beam down in the direction of the solar arrays. This shows that the operation of the Hall thruster does not cause contamination to the spacecraft other than at the top surface where the thruster is located.

This simulation has been computed assuming an initial spacecraft floating potential of 0 V. As already mentioned, fast transients in the potential can influence the distribution of the charge-exchange ions. However, due to our initial assumption of a quasi-neutral plasma

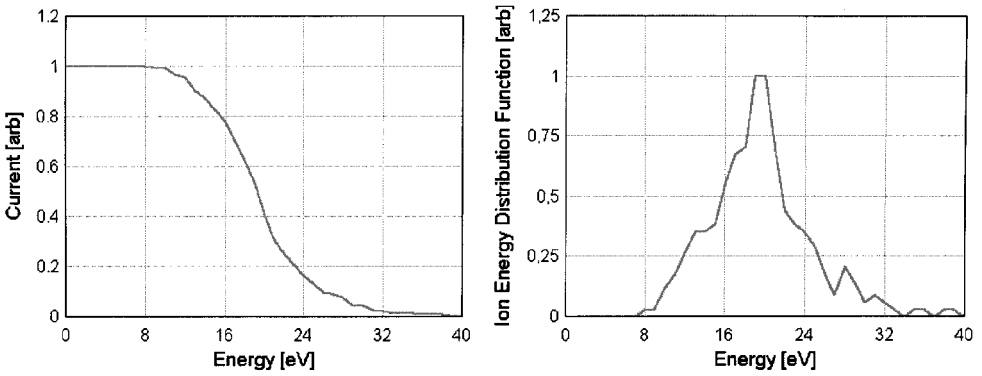

Fig. 12 Virtual EPDP-RPA sensor data.

used to derive the potential distribution, charged surfaces cannot be treated in this code. This would require solving the potential at every time step using the charge density on the grid and the boundary conditions on the surface. This is computationally very expensive.[21] All other simulation surfaces like the solar array were also set to 0 V for the same reason. If flight data reveal fast potential transients and, accordingly, an impact of charge-exchange ions at sensors outside the top surface, a potential solver and a more sophisticated electron model needs to be implemented in the simulation to avoid the quasi-neutrality approach. Because code verifications with ground-test data were successful using the quasi-neutrality assumption,[12] the present numerical model does not address problems related to fast spacecraft floating potential transients.

We will now try to estimate the electric propulsion diagnostic package instrument data that we expect to measure in flight. This package[27] consists of a Langmuir probe, a retarding potential analyser sensor located next to the thruster, and a quartz crystal microbalance (QCM) and solar cell sample mounted on the $-X$ side panel next to the solar arrays. As expected from Fig. 11, there is no interaction from charge-exchange ions with the QCM or solar cell sample (at least in our zero floating potential assumption). However, we can give some useful estimates for the Langmuir probe and RPA sensor.

As we know from Figs. 8 and 10, the backflow ion density is not symmetric around the thruster axis. Because the exact payload location is not fixed yet, we will analyze both extreme cases. The Langmuir probe is located at a radial distance of 470 mm from the thruster axis and approximately 70 mm above the spacecraft surface. At this location, the electron density (quasi-neutral assumption equals charge-exchange ion density) is $n_e = 7 \times 10^{13}$ m^3, plasma potential is $V_p = -2.7$ V at the side where the cathode is located, and $n_e = 5 \times 10^{13}$ m^3 and $V_p = -12.9$ V at the opposite side. Hence, the electron density differs about 40% depending on the instrument location. The electron temperature is fixed in our model to $T_e = 4$ eV throughout the whole simulation domain and can not be computed for a specific location. This value corresponds to beam measurements by Manzella.[7] Because measurements by Kim et al.[9] indicate a smaller electron temperature at lower ion densities (such as at the EPDP location), the actually electron temperature measured by the EPDP Langmuir probe will most probably be below the assumed 4 eV. The negative plasma potential in our simulation is due to our choice of the reference density n_{ref}, which defines where the potential is set to zero. Hence, the real measured plasma potential is expected to be between zero and our reference potential at the thruster's exit, which is 20 V. All plasma parameters (electron density, temperature, plasma potential) appear to be within the design limits of the EPDP Langmuir probe.[27]

We next evaluate the energy distribution from a virtual RPA sensor at the same location as the Langmuir probe (Fig. 12). It is a function of the potential distribution and maximum potential built up in front of the thruster. The data show a peak around 20 eV between 0 and 35 eV. The 20-V peak corresponds to the potential hump in front of the thruster (Fig. 8). These data suggest no sputtering on the spacecraft surface, because aluminium has a sputter threshold of 68 eV. The simulated EPDP instrument data are summarized in Table 4.

Table 4 EPDP instrument simulation results

Parameter	Simulation result
Electron density n_e	5×10^{13}–7×10^{13} m^{-3}
Electron temperature T_e	4 eV (input parameter)
Plasma potential V_p	0–20 V
Charge-exchange energy peak	20 eV

Conclusions

A three-dimensional numerical model based on a hybrid PIC code with MCC was developed to study spacecraft–environment interactions related to ESA's SMART-1 spacecraft. The simulation follows ions and neutrals emitted from a Hall thruster assuming a quasi-neutral plasma to compute the potential. With ground-test data, the ion current and energy distribution could be verified successfully. Charge-exchange ions are generated and analyzed for backflow contamination and distribution around the spacecraft. Virtual instruments are added to compute plasma parameters of interest inside the simulation domain.

The simulation was applied on the SMART-1 geometry, evaluating the influence from operating a Hall thruster. The backflow current to the spacecraft surface was found to be 0.9% of the ion beam current. With a simple estimate, this current would change the spacecraft floating potential at least one order of magnitude below solar-wind-induced floating potentials. The charge-exchange ion distribution was found to be composed of two parts: a cone of backflow ions concentrated inside the inner anode radius area and radially distributed charge-exchange ions. In the presented computations, the charge-exchange ions did not influence the spacecraft other than the top surface where the thruster is located, based on the assumption of a 0-V spacecraft floating potential. During eclipses, fast floating potential transients can occur and the 0-V assumption is not valid any more, limiting the application of this model. Virtual probes were added to the simulation domain representing the EPDP Langmuir and RPA probes. The obtained data were found to be within the respective design limits. The peak charge-exchange energy was found to be around 20 V, which is well below the sputter threshold of aluminium.

In general, the computations did not show any significant interaction of the Hall thruster plasma and the SMART-1 spacecraft. The code seems to be valuable to assist future in-flight data analysis and instrument calibration. A comprehensive validation of space measurements and simulation predictions will lead to a powerful tool to enable mission designers to evaluate the influence of Hall thruster operations onboard a spacecraft.

References

[1] Valentian, D., and Maslennikov, N., "The PPS 1350 Program," IEPC-97-134, Cleveland, OH, Aug. 1997.

[2] Lyszyk, M., Klinger, E., Secheresse, O., Bugeat, J. P., Valentian, D., Cadiou, A., Beltan, T., and Gelas, C., "Qualification Status of the PPS1350 Plasma Thruster," AIAA Paper 99-2278, June 1999.

[3] Racca, G. D., and Foing, B. H., "An Overview on the Status of the SMART-1 Mission," International Academy of Astronautics, IAA-99-IAA.11.2.09, Oct. 1999.

[4]Carruth, M. (ed.), "Experimental and Analytical Evaluation of Ion Thruster/Spacecraft Interactions," Jet Propulsion Lab., Publication 80-92, California Inst. of Technology, Pasadena, CA, 1981.

[5]Tajmar, M., Rüdenauer, F., and Fehringer, M., "Backflow Contamination of Indium Liquid-Metal Ion Emitters (LMIE): Numerical Simulations," IEPC-99-070, Kitakyushu, Japan, Oct. 1999.

[6]Wang, J., Brinza, D. E., Polk, J. E., and Henry, M. D., "Deep Space One Investigations of Ion Propulsion Plasma Environment: Overview and Initial Results," AIAA Paper 99-2971, June 1999.

[7]Manzella, D. H., "Stationary Plasma Thruster Ion Velocity Distribution," AIAA Paper 94-3141, June 1994.

[8]Manzella, D. H., and Sankovic, J. M., "Hall Thruster Ion Beam Characterization," AIAA Paper 95-2927, July 1995.

[9]Kim, S., Foster, J. E., and Gallimore, A. D., "Very-Near-Field Plume Study of a 1.35-kW SPT-100," AIAA Paper 96-2972, July 1996.

[10]King, L. B., "Transport-Property and Mass Spectral Measurements in the Plasma Exhaust Plume of a Hall-Effect Space Propulsion System," Ph.D. Dissertation, Dept. of Aerospace Engineering, Univ. of Michigan, Ann Arbor, MI, May 1998.

[11]Perot, C., Gascon, N., Bechu, S., Lasgorceix, P., Dudeck, M., Garrigues, L., and Boeuf, J. P., "Characterization of a Laboratory Hall Thruster with Electrical Probes and Comparisons with a Two-Dimensional Hybrid Particle-in-Cell Monte Carlo Collision Model," AIAA Paper 99-2716, June 1999.

[12]Oh, D. Y., and Hastings, D. E., "Experimental Verification of a Particle-in-Cell Discrete Simulation Monte Carlo Model for Hall Thruster Plumes," AIAA Paper 96-3196, July 1996.

[13]VanGilder, D. B., and Boyd, I., "Particle Simulations of the SPT-100 Plume," AIAA Paper 98-3797, July 1998.

[14]VanGilder, D. B., Keidar, M., and Boyd, I., "Modeling Hall Thruster Plumes Using Particle Methods," AIAA Paper 99-2294, June 1999.

[15]Birdsall, C. K., and Langdon, A. B., *Plasma Physics via Computer Simulation*, Adam Hilger, New York, 1991.

[16]Birdsall, C. K., "Particle-in-Cell Charged-Particle Simulations, Plus Monte Carlo Collisions With Neutral Atoms, PIC-MCC," *IEEE Transactions on Plasma Science*, Vol. 19, No. 2, 1991, pp. 65–85.

[17]Bareilles, J., Garrigues, L., and Boeuf, J. P., "Modeling of the Plume of a Stationary Plasma Thruster," *Proceedings of the 3rd International Conference on Spacecraft Propulsion*, Centre National d'Etudes Spatiales, ESA, Cannes, France, Oct. 2000.

[18]Bishaev, A., and Kim, V., "Local Plasma Properties in a Hall-Current Accelerator with an Extended Acceleration Zone," *Soviet Physics–Technical Physics*, Vol. 23, Sept. 1978, pp. 1055–1057.

[19]Williams, G. J., Smith, T. B., Gulczinski, F. S., Beal, B. E., Gallimore, A. D., and Drake, R. P., "Laser-Induced Fluorescence Measurement of Ion Velocities in the Plume of a Hall Thruster," AIAA Paper 99-2424, June 1999.

[20]Cedolin, R. J., Hargus, W. A., Jr., Hanson, R. K., and Capelli, M. A., "Laser-Induced Fluorescence Diagnostics for Xenon Hall Thrusters," AIAA Paper 96-2986, July 1996.

[21]Tajmar, M., and Wang, J., "Three-Dimensional Numerical Simulation of Field-Emission-Electric-Propulsion Neutralization," *Journal of Propulsion and Power*, Vol. 16, No. 3, 2000, pp. 536–544.

[22]Haas, J. M., and Gallimore, A. D., "Characterization of the Internal Plasma Structure of a 5 kW Hall Thruster," IEPC-99-078, Kitakyushu, Japan, Oct. 1999.

[23]Rosenberg, D., and Wehner, G. K., "Sputtering Yields for Low Energy He^+-, Kr^+-, and Xe^+-Ion Bombardment," *Journal of Applied Physics*, Vol. 33, No. 5, 1962, pp. 1842–1845.

[24]Rapp, D., and Francis, W. E., "Charge Exchange between Gaseous Ions and Atoms," *Journal of Chemical Physics*, Vol. 37, No. 11, 1962, pp. 2631–2645.

[25]Gnizdor, R., Kozubsky, K., Koryakin, A., Maslennikov, N., Pridannikov, S., Day, M., "SPT100 Life Test with Single Cathode up to Total Impulse Two Million Nanoseconds," AIAA Paper 98-3790, July 1998.

[26]Pedersen, A., "Solar Wind and Magnetosphere Plasma Diagnostics by Spacecraft Electrostatic Potential Measurements," *Annales Geophysicae*, Vol. 13, 1995, pp. 118–129.

[27]Capacci, M., Matticari, G., Noci, G., Severi, A., and Borie, D., "Electric Propulsion Diagnostic Package for the Characterization of the Plasma Thruster/Spacecraft Interactions on STENTOR Satellite," AIAA Paper 99-2277, June 1999.

A. Ketsdever
Guest Associate Editor